GPM DUAL-FREQUENCY RATIO CHARACTERISTICS IN THE MELTING LAYER

Minda Le * and V. Chandrasekar

Colorado State University
1373, campus Delivery
Fort Collins CO 80523-1373, USA

ABSTRACT

The Global Precipitation Measurement (GPM) mission is centered on the deployment of a core observatory satellite with an active dual-frequency precipitation radar (DPR), operating at Ku (13.6 GHz) and Ka (35.5 GHz) band. DPR offers dual-frequency observations along the vertical profile which allow us to investigate the microphysical properties using the difference between the reflectivity at two frequency channels (measured dual frequency ratio or DFRm). The DFRm profiles have different features for different microphysical composition along the vertical profiles. Some of these features are the DFRm maximum value; the DFRm local minimum value; the slope of the DFRm between the maximum and minimum points. In this paper, we characterize these features using both theoretical models and APR2 (airborne precipitation radar generation 2) radar data. The theoretical model and airborne radar data are used to develop classification of dual frequency radar observation of precipitation, such as convective and stratiform profiles, so that the subsequent retrievals can benefit from such a scheme.

Index Terms — GPM, Measured dual-frequency ratio DFRm, Profile classification.

1. INTRODUCTION

The next generation of precipitation radar (PR) is expected to be launched on board the Global Precipitation Measurement (GPM) core satellite in 2013 following the success of the Tropical Rain Measuring Mission (TRMM) launched in 1997 (Iguchi et al 2000). GPM is a science mission with integrated applications goals for advancing the knowledge of the global water/energy cycle variability as well as improving weather, climate, and hydrological prediction capabilities through more accurate and frequent measurements of global precipitation. The GPM core satellite will be equipped with a dual-frequency precipitation radar (DPR) operating at Ku (13.6 GHz) and Ka (35.5 GHz) bands. DPR on aboard the GPM core satellite is expected to improve our knowledge of precipitation processes relative to the single-frequency (Ku band) radar used in TRMM by providing greater dynamic range, more detailed information on microphysics, and better accuracies in rainfall and liquid water content retrievals. New Ka band channel observation of DPR will help to improve the detection thresholds for light rain and snow relative to TRMM (Iguchi et al. 2002). The dual-frequency returns will allow us to better distinguish regions of liquid, frozen, and mixed-phase precipitation.

In Le et al. (2009), it was shown that the difference between the reflectivity at two frequency channels or DFRm is well suited for profile classification for GPM DPR. The DFRm profiles have different features for different microphysical composition along the vertical profiles. Some of these features could be the DFRm maximum value; the DFRm local minimum value; the slope of the DFRm between the maximum and minimum points. This paper is focused on characterizing these features towards potential implication for microphysical retrievals.

In order to verify that different microphysics have different features on DFRm profile, we study these features mentioned above using both theoretical models and APR2 radar data of NAMMA (NASA African Monsoon Multidisciplinary Analysis)

experiment. The theoretical model and airborne radar data are used to drive profile classification of dual frequency radar observation of precipitation, such as convective and stratiform profiles, so that the subsequent retrievals can benefit from such a scheme.

2, Background of measured dual frequency ratio DFRm

DPR offers two independent observations from two frequency channels. Although measurements at both frequencies suffer from attenuation when radar beam propagating through rain and melting region (Bringi and Chandrasekar 2001), attenuation from Ka band is larger than Ku band. DFRm (in dB scale) is defined as

$$\mathrm{DFR_m} = \mathrm{Z_m}(\mathrm{K_u}) - \mathrm{Z_m}(\mathrm{K_a}) \tag{1}$$

$\mathrm{Z_m}$ (in dBZ) is the measured radar reflectivity. $\mathrm{Z_m}$ in linear scale (denoted as $\mathrm{Z_{m,lin}}$) can be related to effective reflectivity factor $\mathrm{Z_{e,lin}}$ through

$$\begin{aligned}\mathrm{Z_{m,lin}} &= \mathrm{Z_{e,lin}} \times \mathrm{A} \\ &= \mathrm{Z_{e,lin}} \exp[-0.2\ln(10) \int_0^{\mathrm{r}} \mathrm{k(s)ds}]\end{aligned} \tag{2}$$

Where A is the attenuation factor from radar to the bin of interest. $\mathrm{Z_{e,lin}}$ which is related to the drop size distribution N(D) and the backscatter cross section σ_b of the hydrometeors for an incident wavelength λ, is given as

$$\mathrm{Z_{e,lin}} = \frac{\lambda^4}{\pi^5 |\mathrm{K_w}|^2} \int_0^\infty \mathrm{N(D)} \sigma_\mathrm{b}(\mathrm{D}, \lambda) \mathrm{dD} \tag{3}$$

$\mathrm{K_w}$ is the dielectric constant of water and $|\mathrm{K_w}|^2 \cong 0.93$. Natural variation of drop size distribution N(D) can be approximated by a Gamma model (Ulbrich 1983) as

$$\mathrm{N(D)} = \mathrm{N_w f}(\mu) \left(\frac{\mathrm{D}}{\mathrm{D_0}}\right)^\mu \exp\left[-(3.67+\mu)\frac{\mathrm{D}}{\mathrm{D_0}}\right],$$

$$\mathrm{f}(\mu) = \frac{6}{(3.67)^4} \frac{(3.67+\mu)^{\mu+4}}{\mathrm{r}(\mu+4)} \tag{4}$$

Where $\mathrm{D_0}$ (mm) is the medium volume diameter, μ is a measurement of shape of drop size distribution and $\mathrm{N_w}(\mathrm{mm^{-1}m^{-3}})$ is the normalized intercept parameter of an equivalent exponential distribution with the same water content and $\mathrm{D_0}$. Take log scale of both sides, (2) can be expressed as

$$\mathrm{Z_m} = \mathrm{Z_e} - \log_{10}(\exp[0.2\ln(10) \int_0^{\mathrm{r}} \mathrm{k(s)ds}]) = \mathrm{Z_e} - \mathrm{PIA} \tag{5}$$

PIA (in dB) denotes the two-way attenuation from radar to the bin of interest. $\mathrm{Z_e}$ is the dB scale of $\mathrm{Z_{e,lin.}}$ K is specific attenuation in dB per kilometer, related to drop size distribution N(D) and extinction cross section σ_{ext} of the hydrometeors

$$\mathrm{k} = 4.343 \times 10^3 \int_0^\infty \mathrm{N(D)} \sigma_{\mathrm{ext}}(\mathrm{D}, \lambda) \mathrm{dD} \tag{6}$$

Radar dual-frequency ratio (DFR) in dB, describing the difference of reflectivity factor between two frequency channels, is defined as

$$\mathrm{DFR} = \mathrm{Z_e}(\mathrm{K_u}) - \mathrm{Z_e}(\mathrm{K_a}) \tag{7}$$

Substituting from which one can obtain

$$DFR_m = Z_m(K_u) - Z_m(K_a) = DFR + \delta PIA \tag{8}$$

$\delta\,\mathrm{PIA}$ is the attenuation difference between Ku- and Ka- band expressed in dB scale. It is a positive number since Ka band attenuation is larger than Ku band. From (8), it is easy to see that DFRm is composed of two parts: a) DFR caused by the non-Rayleigh scattering of precipitation particles; and b) $\delta\,\mathrm{PIA}$ which is responsible for the power loss due to attenuation.

Figure 1 shows typical vertical profile of DFRm and its corresponding reflectivity profiles for stratiform and convective rain respectively. Stratiform and convective rain has different microphysics along vertical profile, comparing figure 1 (b) and (d), it is not hard to observe for the two cases that the shape of DFRm profile has different features A schematic plot of DFRm is illustrated in figure 2 to involve the key points that

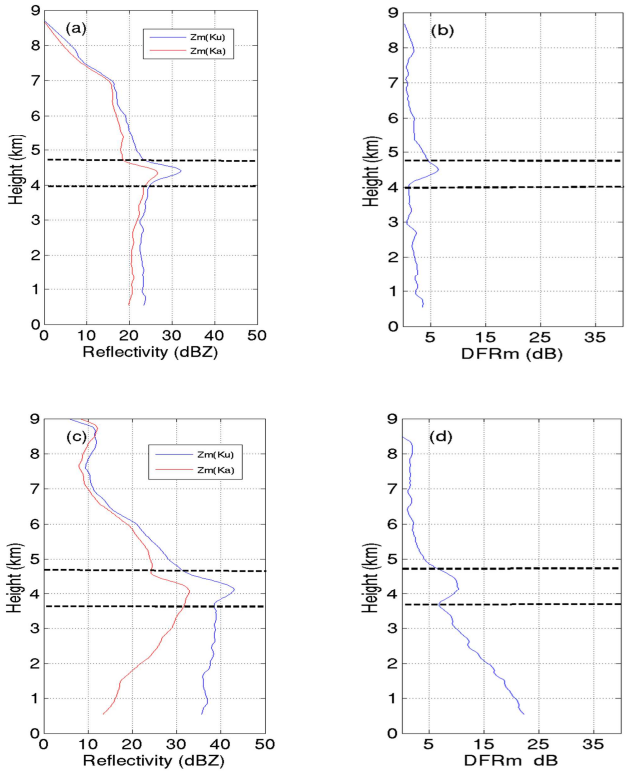

Figure 1, Typical vertical profile for stratiform (a)(b) and convective (c)(d) rain from NAMMA APR2 data; (a)(c) Reflectivity at Ku and Ka band; (b)(d) DFRm. Dashed line are estimated melting layer top and bottom using criteria from Le and Chandrasekar (2011).

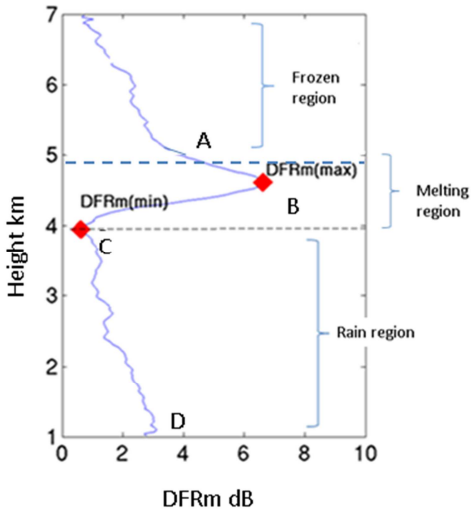

Figure 2, Schematic plot of DFRm profile with key point A, B, C and D. Point A: slope of DFRm has maximum. Point B: maximum of DFRm. Point C: local minimum of DFRm. Point D: DFRm value near surface.

could be estimated to study the characteristics of DFRm. These key points include the maximum slope of DFRm (point A); maximum value of DFRm (point B); local minimum value of DFRm (point C) and DFRm value toward surface (point D). The value of these four points and the slope of DFRm between point B and C, C and D are studied. The slope between point B and C is defined as the difference of DFRm value at two points respect to the difference of height. The same definition applies to the slope between point C and D. The dashed lines in figure 1 are melting layer regions detected using criteria described in Le and Chandrasekar (2011). Melting layer top was detected using the height at which slope of DFRm hits maximum value (point A in figure 2). Melting layer bottom was detected using the height at which DFRm has local minimum value (point C in figure 2). The DFRm criteria showed good comparisons with other existing criteria such as linear depolarization ratio (LDR) and Doppler velocity.

The shape of DFRm in figure 1(b) and (d) has some common features. Above melting layer top, DFRm values are small and increase slightly with the decrease of height. Entering the melting region, DFRm increases sharply till it hits a maximum value, then it decreases obviously with decreasing height till it reaches a local minimum value. This “bump” of DFRm is associated with “aggregate” and “breakup” process in melting layer. Below local minimum value, DFRm keeps increasing. However, comparing figure 1(b) and (d), obvious differences are 1) DFRm value at point B is larger for convective rain than stratiform rain; 2) The slope between point B and C is larger (steeper) for stratiform rain than convective rain; 3) DFRm value at point C is larger for convective rain than stratiform rain; 4) The slope between point C and D is larger (steeper) for convective rain than stratiform rain. 5) DFRm value toward surface is much larger for convective rain than stratiform rain. In order to verify that these are typical features of DFRm for different rain types, APR2 observations are studied in section 3.

3, Study of characteristics of DFRm using Airborne Precipitation radar (APR2) observation

Figure 3 illustrates a sample plot of APR2 measurements at nadir during NAMMA campaign.

From top to bottom panels, are measured reflectivity at Ku, Ka bands, DFRm, Linear Depolarization Ratio (LDR) at Ku band and Doppler velocity at Ku band. Due to the fine vertical resolution (30m), melting layer can be seen clearly from the reflectivity measurements.

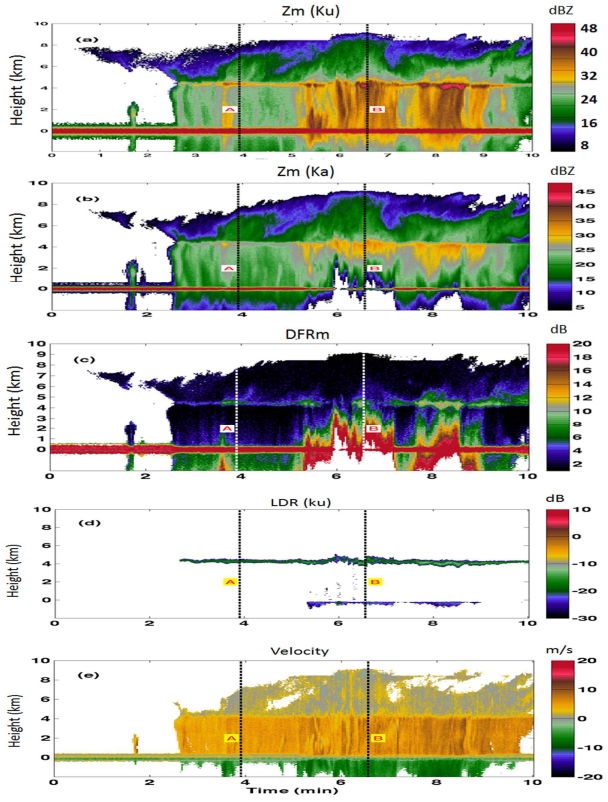

Figure 3, Measurements of APR2 NAMMA data 20060903-142134 at nadir. (a) Measured reflectivity at Ku band; (b) Measured reflectivity at Ka band; (c) Measured dual-frequency ratio (DFRm); (d) Linear Depolarization ratio (LDR) at Ku band; (d) Doppler velocity at Ku band.

To study the characteristics of DFRm profile for different rain types, all NAMMA data are classified into stratiform, convective and other rain types using the combined information from TRMM-like algorithm (Awaka et al 1997) as well as velocity. Five DFRm characteristics mentioned in section 2 are studied. All five characters match well with the findings from figure 1. Histogram of melting layer width detected by DFRm criteria is wider for convective rain than stratiform rain which is a reasonable result.

4, Study of characteristics of DFRm using theoretical models

Theoretical simulation provides a way to study the impact of various factors to the DFRm such as particle density, scattering model for melting particles, drop size distribution etc. Meanwhile, impact from two aspects of DFRm namely DFR and δ PIA can be studied separately.

The following summarizes results of theoretical simulations to understand the DFRm profiles.

For convective rain, due to riming process, the density of scattering particles in both frozen and melting regions are higher than stratiform rain. In order to study the effect of snow density to DFRm, a D0 and Nw vertical profile is assumed, density of dry snow is changed from 0.1 g/cm^3 to 0.4 g/cm^3. From simulated profiles, it was found that DFR is not sensitive to snow density change. Different DFRm curves are controlled by attenuation difference δPIA. δPIA is relative small above melting region (< 1dB for dry snow density of 0.4 g/cm3). δPIA increases obviously within melting layer and particles with higher density introduce more attenuation difference than particles with lower density. Therefore, peak value of DFRm (point B), local minimum value of DFRm (point C) and DFRm value toward surface (point D) are larger for scattering particles at higher density such as the case for convective rain.

Drop size distribution is another factor that influences DFRm profile. In order to test the effect of drop size to DFRm, medium drop size diameter Do profile is set to be varied while keeping Nw same as before. Dry snow density is fixed at 0.1 g/cm^3. From simulation results, it was found that both DFR and δPIA are affected by Do change. Larger Do results in larger DFR and δPIA values. δPIA is more sensitive to Do change compared to DFR especially within rain region. Combining two aspects, DFRm profile shows smaller slope between DFRm maximum and local minimum value (B, C slope in figure 2) and larger slope between DFRm local minimum and surface value (C, D slope in figure 2) for profile with larger Do values. Nw represents particle number concentrations. The effect of Nw change to

DFRm profile is studied assuming Nw (in log scale) is varied while keeping Do the same. From simulation results, it was found that DFR is not affected by Nw change since DFR represents a ratio. DFRm profile is controlled by δPIA which is affected much by Nw. Combining two aspects, DFRm profile shows smaller slope between DFRm maximum and local minimum value (B, C slope in figure 2) and larger slope between DFRm local minimum and surface value (C, D slope in figure 2) for profile with larger Nw values. As we know, by increasing either Do or Nw in drop size distribution, total water content increases. Therefore, DFRm profile shows smaller slope between DFRm maximum and local minimum value (B, C slope in figure 2) and larger slope between DFRm local minimum and surface value (C, D slope in figure 2) for profile with larger water content such as the case for convective rain.

Theoretical simulation is performed using an overpass of DSD parameters retrieved from a NAMMA overpass 20060903_142134 shown in figure 3 using retrieval algorithm described in Le et al. (2009). Melting region is detected using LDR threshold. Rain type is classified by TRMM-like method and velocity information. Different scattering models are used to model different rain types. Histogram of five key characteristics of DFRm profile mentioned in section 2 are studied and compared with radar observations from APR2 data. All five characteristics of DFRm for stratiform and convective rain match with each other.

Therefore, from both theoretical simulation and APR2 radar observations, features of DFRm profile for different microphysics are characterized and verified.

5, Summary

Vertical profile of measured dual frequency ratio (DFRm) is studied for GPM profile classification using both APR2 radar observation and theoretical simulation. Different features of DFRm are characterized for different microphysics along vertical profile. These features include peak value of DFRm; slope of DFRm between peak and local minimum value; local minimum value of DFRm; slope of DFRm between local minimum and toward surface value; DFRm value toward surface. Histogram of these five key features of DFRm from APR2 observations show good consistency with theoretical results for both stratiform and convective rain types. The study of DFRm characteristics in this paper is used to derive classification of dual frequency radar observation of precipitation, such as convective and stratiform profiles, so that the subsequent retrievals can benefit from such a scheme.

ACKNOWLEDGEMENT

This research is supported by the NASA GPM/PMM program.

REFERENCES

C. W. Ulbrich, 1983: Natural variation in the analytical form of the raindrop-size distribution. *J.Climate Appl. Meteor.*, vol. 22, no. 10, pp.1764-1775.

J. Awaka, T. Iguchi, H. Kumagai, and K. Okamoto, 1997: Rain type classification algorithm for TRMM precipitation radar. *Proc. IEEE IGARSS 1997*, pp.317-319.

M. Le, V. Chandrasekar and S. Lim, 2009: Microphysical retrieval from dual-frequency GPM observations. *34th AMS radar conference*, Williamsburg, Oct 5-9.

M. Le and V. Chandrasekar,2011: Precipitation type and profile classification for GPM-DPR. IGARSS 2011', Vancouver, July.

T. Iguchi, T. Kozu, R. Meneghini, J. Awaka, and K. Okamoto, 2000: Rain-profiling algorithm for the TRMM Precipitation Radar. *J. Appl. Meteorol*., vol. 39, pp. 2038-2052.

T. Iguchi, R. Oki, A. Eric and Y. Furuhama, 2002: Global precipitation measurement program and the development of dual-frequency precipitation radar. *J. Commun. Res. Lab. (Japan)*, 49, 37-45.

V. N. Bringi and V. Chandrasekar, 2001: Polarimetric Doppler Weather Radar-Principles and Applications. Cambridge University Press.